JOC The Journal of Organic Chemistry

pubs.acs.org/joc Article

Structure–Photoreactivity Studies of BODIPY Photocages: Limitations of the Activation Barrier for Optimizing Photoreactions

Komadhie C. Dissanayake,[‡] Ding Yuan,[‡] and Arthur H. Winter*

Cite This: *J. Org. Chem.* 2024, 89, 6740–6748 Read Online

ACCESS | Metrics & More | Article Recommendations | Supporting Information

ABSTRACT: BODIPY photocages are photoreactive chromophores that release covalently linked cargo upon absorption of visible light. Here, we used computations of the T_1 photoheterolysis barrier to ascertain whether a computational approach could assist in *a priori* structure design by identifying new structures with higher quantum yields of photorelease. The electronic structure–photoreactivity relationships were elucidated for boron-substituted and core-functionalized 2-substituted BODIPY photocages as well as aryl substitutions at the *meso*-methyl position. Although there is a clear trend for the 2-substituted derivatives, with donor-substituted derivatives featuring both lower computed barriers and higher experimental quantum yields, no trend in the quantum yield with the computed activation barrier is found for the *meso*-methyl-substituted or boron-substituted derivatives. The lack of a correlation between the experimental quantum yield with the computed barrier in the latter two substitution cases is attributed to the substituents having larger effects on the rates of competing channels (internal conversion and competitive photoreactions) than on the rate of the photoheterolysis channel. Thus, although in some cases computed photoreaction barriers can aid in identifying structures with higher quantum yields, the ignored impacts of how changing the structure affects the rates of competing photophysical/photochemical channels limit the effectiveness of this single-parameter approach.

INTRODUCTION

Photocages, or photolabile protecting groups (PPGs), allow the activation of biomolecules using light as a stimulus with high spatiotemporal control.[1−5] Unlike popular PPGs like the phenacyl,[6,7] *o*-nitrobenzyl moiety,[8,9] or coumarin PPGs,[10] which absorb predominantly UV light, BODIPY PPGs absorb visible light and even near-infrared light, ideal for biological studies.[11−16]

A desirable property of PPGs is a high uncaging efficiency, which provides a reduced irradiation time to achieve photorelease and fewer background photoreactions. The uncaging efficiency is the product of the extinction coefficient at the irradiation wavelength and the release quantum yield (Φ_r). Although BODIPY PPGs have high extinction coefficients (40,000−200,000 M^{-1} cm^{-1} at the λ_{max} is typical), the Φ_r's for the first-generation BODIPY PPGs were lower than the Φ_r's for the best UV-absorbing PPGs.[17,18]

Several strategies have been undertaken to alter the structure to improve the Φ_r of first-generation BODIPY PPGs. Because a photoreaction quantum yield depends on the ratio of the rate of the desired photoreaction over the sum of the rates of all possible channels, the quantum yield can be improved by either increasing the photoreaction rate constant or diminishing the rate constants of the competitive excited-state channels (internal conversion, ion pair recombination, undesired photochemistry, etc.). One way to diminish the rate of internal conversion is to force the photoreaction to the triplet state, which is longer-lived compared to the singlet state, because internal conversion and luminescence are spin forbidden. Achieving intersystem crossing (ISC) was accomplished by appending bromine or iodine atoms to the BODIPY core, which accelerates ISC to the triplet state via the heavy atom effect and leads to higher Φ_r.[19] Additionally, modifications to thwart unproductive channels, such as internal conversion or ion pair recombination, have been undertaken by rigidifying the BODIPY structure or stabilizing the cation to prevent ion pair recombination, or by adding internal cation traps.[20,21]

Less obvious is how to improve the rate of the desired photorelease photoreaction, because the conventional structure–reactivity rules for thermal S_N1 reactions do not apply to photo-S_N1 reactions. Here, we attempted to rationally improve the photoreaction rate by computing the triplet excited-state photoheterolysis activation barrier for varying BODIPY PPGs substituted at the core 2-position, at the boron, and at the exocyclic carbon appended to the *meso* position to evaluate whether computations can make useful structure–reactivity predictions.

We anticipated that BODIPY PPGs with lower computed activation barriers for photoheterolysis would have a larger excited-state heterolysis rate constant and subsequently a higher

Received: December 28, 2023
Revised: March 27, 2024
Accepted: April 17, 2024
Published: May 2, 2024

https://doi.org/10.1021/acs.joc.3c02980
J. Org. Chem. 2024, 89, 6740−6748

Φ_r. We find that this is indeed the case for substitutions at the 2-position. Appending the 2-position of the BODIPY PPG with electron donating groups, which are computed to have lower activation energies, leads to higher Φ_r, whereas withdrawing groups, which are computed to have higher activation barriers, have lower Φ_r. In contrast, similar predictions made for substitutions at the boron of the BODIPY PPG or at the exocyclic *meso* carbon position failed to lead to a similar relationship, which we attributed to the chemical substitution having a greater impact on alternative excited-state channels than the photoreaction channel. Thus, although the activation barrier was predictive for the 2-position, it was unhelpful for the boron-substituted and *meso*-methyl-substituted cases, making this single-parameter approach insufficient as a general photoreactivity predictor for BODIPY PPGs and suggesting that a more sophisticated approach is needed to even make crude photoreactivity predictions.

RESULTS AND DISCUSSION

Effect of Boron Substitution on the Photophysics and Photochemical Efficiencies of BODIPY PPGs (1): Only Alkyl Groups Are Better. A series of boron-substituted BODIPY PPGs were synthesized by reacting **1-F** with a Lewis acid and a nucleophilic reagent of interest, which were chosen to encompass a broad range of electronic properties. As illustrated in Figure 1 and Table 1, the absorption maxima of these derivatives closely coincide (517−526 nm) irrespective of the electronic nature of the substituent at the boron, indicating a lack of significant participation of the boron substituent on the BODIPY chromophore. However, small but significant variations in the emission maxima are observed (529−556 nm), indicating that the substituents do have a small effect on the S_1 energies.

To correlate the electronic nature of the unconjugated substituents to the efficiency of the photocages, the computed triplet energy barrier (T_1, $\Delta E^{\ddagger}$), and the experimental Φ_r's were plotted against Hammett meta (σ_m) values, depicted in Figure 2 (a simplified version can be found in Figure S5).

The DFT-computed energy barrier for T_1 C−O bond breaking decreases with increasing electron-donating properties of the substituent. Although no correlation between the experimental Φ_r and σ_m values is apparent, there is a significant difference changing from electron-withdrawing to inductive electron-donating groups. All the derivatives except **1-CH$_2$TMS** have a positive σ_m, and notably, they exhibited comparable Φ_r's ranging from 0.08 to 0.31, whereas **1-CH$_2$TMS** exhibited a Φ_r of 6.3%, a 41-fold increment of Φ_r compared to the parent BODIPY **1-F**. The results support the hypothesis that increasing electron density improves Φ_r, which also agrees with previously reported BODIPY photocages with methyl and ethyl groups with ∼45 and ∼30-fold increments, respectively, compared to their fluorinated analog.[19]

But the lack of significant changes in Φ_r for the eight other derivatives suggests that the dominant effect of boron substitution on Φ_r is not driven by the excited-state heterolysis barrier. Rather, some other effect is likely operating. For example, it is known that there is a competitive B−R bond excited-state breaking pathway for BODIPY compounds.[22,23] This photoreaction channel is potentially invisible if the bond can thermally reform, but it introduces a light-wasting channel. Perhaps with a B-alkyl group (e.g., Me), this invisible light-wasting photoreaction channel is less efficient (although not zero[22,24]), leading to an increase in the Φ_r.

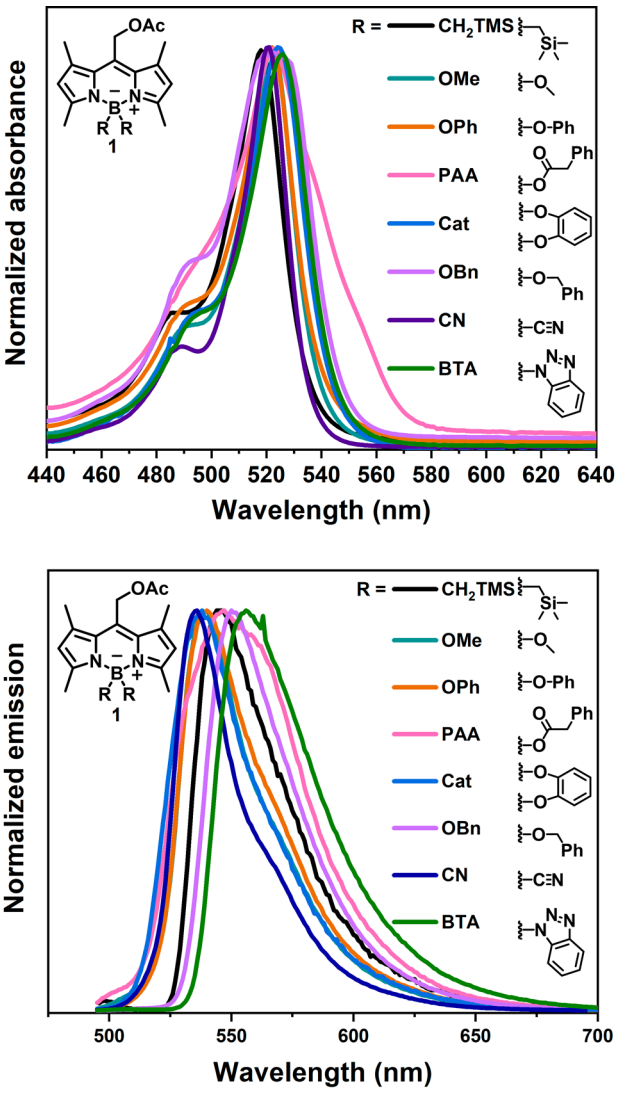

Figure 1. Normalized absorbance (top) and emission (bottom) spectra of boron-substituted BODIPYs in DCM.

Effect of 2-Substituents on Photophysics and Photochemical Efficiencies of BODIPY PPGs (2): Pi-Donating Groups Are Better. A recent report by Weinstain and coworkers demonstrated a correlation between the electron-donating/-withdrawing ability of the substituents at the 2- and 6-positions of BODIPY PPGs with the Φ_r of the BODIPY photocages. 2,6-Disubstitutions with withdrawing groups (e.g., SO_3^-) shut down the photoreaction completely.[25] Although not synthesized in that paper, pi-donating groups in these positions were computed to have smaller T_1 C−O cleavage activation barriers, suggesting the possibility that such pi-donating derivatives would be more photoreactive.

To explore this computed structure−reactivity relationship experimentally, a set of 2-substituted BODIPY PPGs were synthesized (Table 2). To synthesize these derivatives, the parent BODIPY PPG **1-F** was formylated followed by Baeyer villager esterification, hydrolysis, and methylation to provide BODIPY derivatives featuring aldehyde, ester, hydroxyl, and ether groups substituted at the 2-position.

The absorbance and emission spectra of the 2-substituted BODIPY PPGs are shown in Figure 3. EDGs generally induced a red shift in absorbance and emission spectra compared to those

https://doi.org/10.1021/acs.joc.3c02980
J. Org. Chem. 2024, 89, 6740−6748

Table 1. Photophysical and Photochemical Properties of Boron-Substituted (1) Compounds

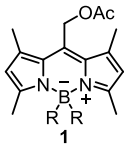

1

compound	R	λ_{ab} (nm)	λ_{em} (nm)	ε ($\times 10^4$ $M^{-1}cm^{-1}$)	Φ_r (%)[b]	$\varepsilon\Phi$ (M^{-1} cm^{-1})
1-Me	Me	519	556	6.1	6.30[a]	3842
1-CH_2TMS	CH_2TMS	518	546	7.6	5.74	4362
1-F	F	517	529	7.1	0.14[a]	99
1-OMe	OMe	522	540	4.0	0.20	80
1-Ph	phenol	522	540	9.2	0.31	285
1-OBn	BnOH	522	550	7.2	0.08	58
1-PAA	phenylacetic acid	523	547	10.0	0.08	80
1-Cat	catechol	524	538	5.9	0.12	71
1-BTA	benzotriazole	526	556	5.5	0.10	55
1-CN	CN	521	536	4.6	0.08	37

[a]Values reported previously.[19] [b]Quantum yields (Φ_r's) were obtained using quantitative ^{1}H NMR following the growth of AcOH in $CDCl_3$/MeOD 1:1 solution with **1-F** as the actinometer. All the samples were irradiated using a LED illuminator at 525 nm in air without purging.

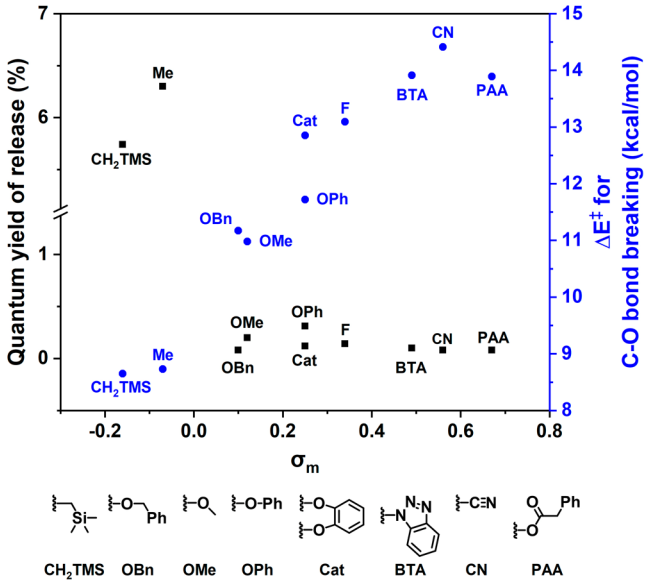

Figure 2. Observed Φ_r and computed T_1 C−O bond breaking energy (B3LYP/6-31+G(d,p), SMD = H_2O) for boron-substituted BODIPYs as plotted versus σ_m Hammett constants. Note that the *Y* axis for Φ_r is truncated to plot the Me and CH_2-TMS derivatives, and the *Y* axis for C−O bond breaking starts at 8 kcal/mol and not 0.

of **1-F**. For example, **2-OH** bearing a hydroxy group features a λ_{max} of 542 nm, a red-shift of 23 nm compared to **1-F**. Additionally, an increase in electron density corresponded to a decrease in the fluorescence intensity and broadening of emission bands. To evaluate the structure−photoreactivity relationship, theoretical $\Delta E^{\ddagger}$ was plotted against Hammett σ_p values and the experimental Φ_r to visualize the correlation between the electron-donating/-withdrawing properties of the 2-substituent on the Φ_r (see Figure 4).

This Hammett plot shows that increasing the electron density enhances the experimental Φ_r while also reducing the theoretical $\Delta E^{\ddagger}$. Both observations suggest that increasing the electron density improves the photo uncaging efficiency in BODIPY photocages by increasing the photoheterolysis rate. The observed results can be further substantiated by referencing specific evidence from the existing literature. As noted previously, Weinstain and co-workers reported the absence of photouncaging when sulfonic acid was substituted in the 2-position, a strong electron-withdrawing group.[25] In work published by our group, it was shown that attaching a weakly donating alkyl group to the core had a minimal impact on Φ_r.[18] Furthermore, the introduction of halogens has resulted in a significant improvement in the Φ_r, but this was attributed to the heavy atom effect promoting ISC rather than an effect on the heterolysis barrier.[19]

To enhance the electron-donating ability of the substituent, **2-OH** was treated with NaOH to deprotonate the hydroxyl group. As observed via UV−visible spectroscopy, the deprotonation process, which is reversible upon acidification, leads to a bathochromic shift upon the addition of base, shown in Figure 5, with an absorption tail that extends into the near-IR. However, attempts to achieve complete deprotonation with excess base led to undesirable hydrolysis of the ester leaving group, thereby impeding the Φ_r experiments. Another noteworthy observation is that **2-OH** and **2-OMe** exhibited a concentration-dependent release efficiency, where higher concentrations showed a noticeable decrease in release efficiency, suggesting the possibility of aggregates.

***meso*-Methyl Aryl Substituents Attenuate Φ_r despite Having Lower Computed T_1 C−O Heterolysis Barriers.** In prior investigations, it was shown that the attachment of a *meso*-methyl group surprisingly shut down the photorelease reaction.[19] In contrast, Szymański and co-workers found that substituting the BODIPY PPG with a *meso*-methyl allyl group improved the relative rate of release compared to the H-substituted derivative by up to ∼7-fold.[21] These authors attributed the improvement in the Φ_r to the stabilization of the carbocation through resonance, slowing the light-wasting recombination of the contact ion pair and giving additional time for the desired solvent separation and trapping.

In this study, we examined the effect of an aryl group at the *meso*-methyl position on Φ_r, considering the well-known stability of benzylic carbocations through resonance and the ability to alter the donating ability of the aryl group with *para* substituents. Accordingly, two *meso*-methyl aryl BODIPY derivatives were synthesized by reacting the corresponding Grignard reagent with compound **5** followed by attaching the acetic acid leaving group via DCC coupling (a third derivative

https://doi.org/10.1021/acs.joc.3c02980
J. Org. Chem. 2024, 89, 6740−6748

Table 2. Photophysical and Photochemical Properties of 2- Substituted (2) Compounds

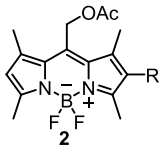

compound	R	λ_{ab} (nm)	λ_{em} (nm)	ε ($\times 10^4$ M^{-1} cm^{-1})	Φ_r (%)[b]	$\varepsilon\Phi_r$ (M^{-1} cm^{-1})
1-F	H	517	529	7.1	0.14[a]	99
2-CHO	CHO	516	531	6.03	0.05	27
2-OCHO	OCHO	527	541	7.20	0.11	79
2-OH	OH	542	609	4.49	0.53	239
2-OMe	OMe	538	610	6.04	0.16	99
2-CH=C(CN)$_2$	CH=C(CN)$_2$	533	561	8.80	0.03	29

[a]Values reported previously.[19] [b]Quantum yields (Φ_r's) were obtained using quantitative ^{1}H NMR following the growth of AcOH in $CDCl_3$/MeOD 1:1 solution with **1-F** as the actinometer. All the samples were irradiated using an LED illuminator at 525 nm in air without purging.

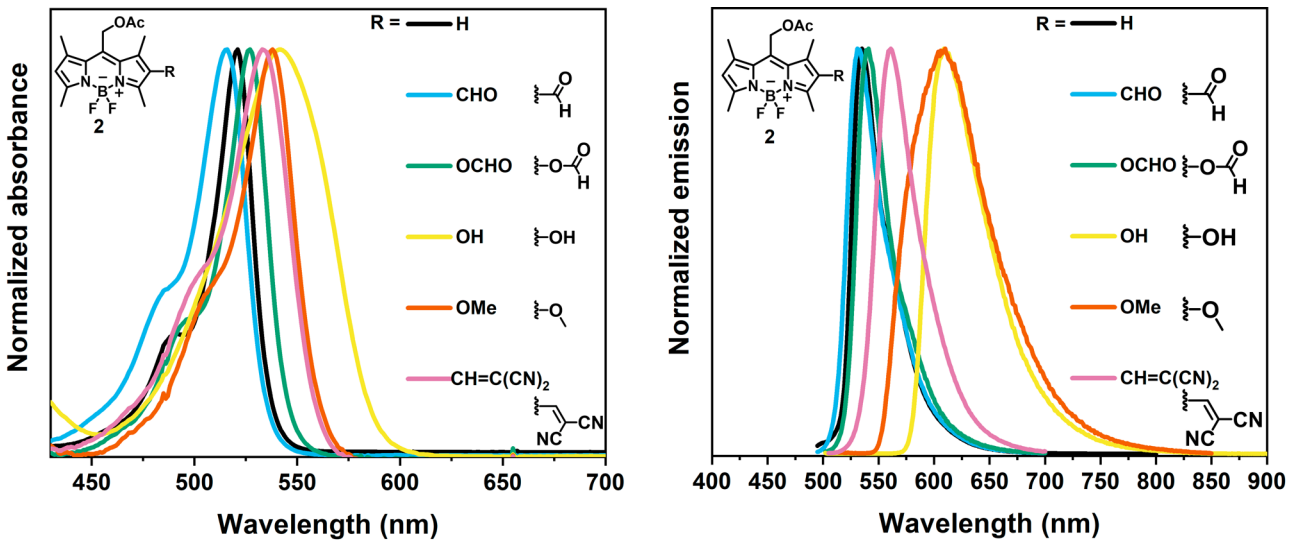

Figure 3. Normalized absorbance and emission spectra of 2-substituted BODIPYs in DCM.

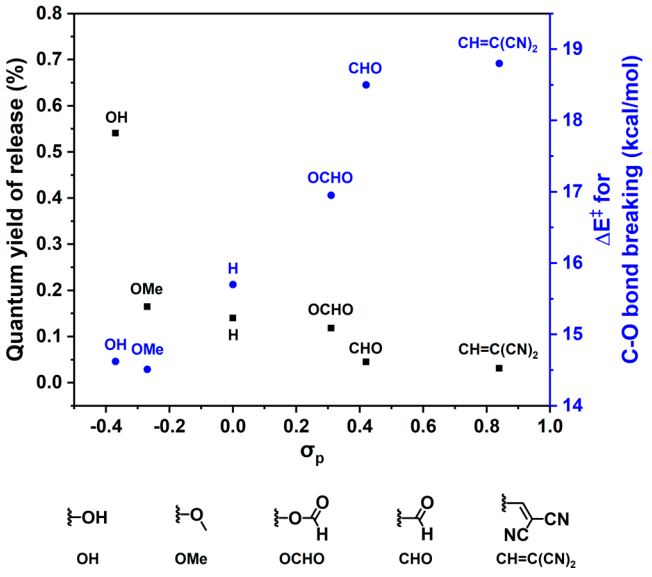

Figure 4. Observed Φ_r and computed T_1 energy barrier ($\Delta E^{\ddagger}$, B3LYP/6-31+G(d,p), SMD = H_2O) for C−O bond breaking for core 2-substituted BODIPYs plotted versus σ_p Hammett constants.

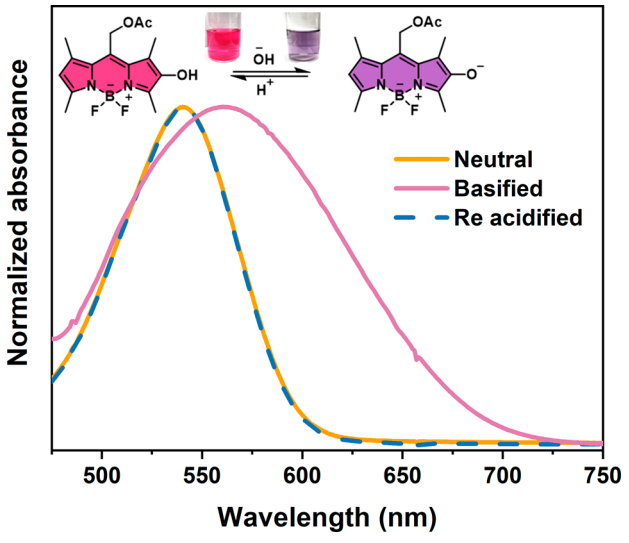

Figure 5. Absorbance spectra demonstrate the deprotonation of **2-OH** upon addition of 0.1 M NaOH and reversal with 0.1 M HCl in MeOH.

prepared in a similar fashion, bearing a *p*-NMe_2-Ph group, proved to be thermally unstable).

https://doi.org/10.1021/acs.joc.3c02980
J. Org. Chem. 2024, 89, 6740−6748

Table 3. Photophysical and Photochemical Properties of *meso*-Methyl-Substituted Compounds

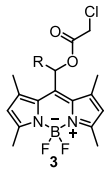

compound	R	λ_{ab} (nm)	λ_{em} (nm)	ε (x10^4 M^{-1} cm^{-1})	Φ_r (%)[a]	$\varepsilon\Phi_r$ (M^{-1} cm^{-1})
3-H	H	524	534	7.36	0.22	165
3-Ph	phenyl	523	543	7.11	0.10	73
3-PhOMe	anisole	522	551	7.08	0.12	82

[a]Quantum yields (Φ_r's) were obtained using quantitative ^{1}H NMR following the growth of chloroacetic acid in $CDCl_3$/MeOD 1:1 solution with **1-F** as the actinometer. All the samples were irradiated using a LED illuminator at 525 nm in air without purging.

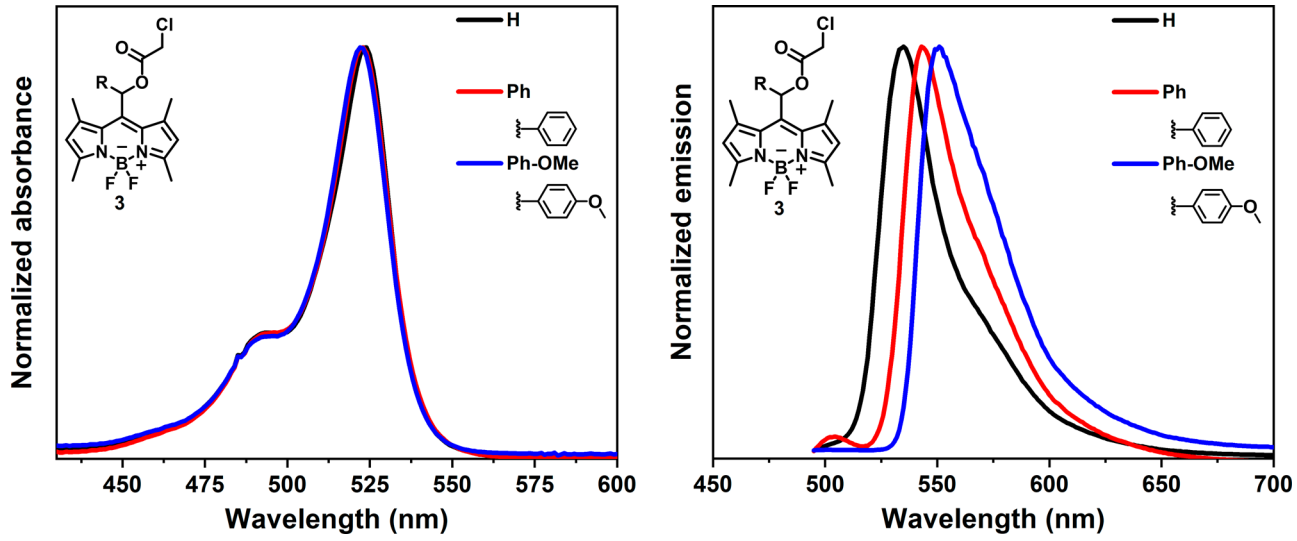

Figure 6. Normalized absorbance and emission spectra of *meso*-methyl-substituted BODIPYs.

A small technical challenge in determining the photorelease of the *meso*-methyl-substituted derivatives had to be overcome. Introducing aryl derivatives to the exocyclic *meso* carbon broadened the ^{1}H NMR signals for the methyl groups at positions 1 and 7. Thus, distinguishing photoreleased AcOH signals by ^{1}H NMR became challenging because of the overlap of the AcOH ^{1}H NMR signal with these broadened methyl peaks. To address this challenge, chloroacetic acid was chosen as the leaving group to avoid spectral overlap of these protons. The photophysical and photochemical properties of the synthesized compounds are presented in Table 3. Figure 6 shows the absorbance and emission spectra for the synthesized *meso*-methyl aryl compounds. The absorbance spectra of the three derivatives have similar maximum absorption wavelengths. Surprisingly, some differences were observed in the emission spectra (534−551 nm), suggesting the involvement of the unconjugated phenyl groups in S_1. Perhaps the aryl rings adopt a conformation, placing the aryl rings over the BODIPY chromophore in S_1 and enabling electronic communication and S_1 stabilization.

The computed $\Delta E^{\ddagger}$ values for T_1 (the first triplet excited state) **3-H**, **3-Ph**, and **3-PhOMe** are 11.2, 8.7, and 7.5 kcal/mol, respectively, making us anticipate higher Φ_r values with the attached aryl rings. However, as shown in Table 3, Φ_r values for the **3-Ph** and **3-PhOMe** were unexpectedly lower than those for **3-H**. This is surprising given our computations and the previous results by Szymański et al. reported for the *meso*-methyl allyl derivatives.

One possible cause for the diminishment in the photoreactivity of **3-Ph** and **3-PhOMe** we considered is that the methyl groups on the 1- and 7- positions may prevent an effective conjugation of the larger aryl ring to the BODIPY core to exert stabilization through resonance. This effect may not be as apparent for the smaller allyl derivative. A supplementary computational analysis was conducted without 1,7-methyl groups to evaluate their impact on the T_1 bond-breaking barrier. However, the computations revealed no significant difference in the energy barrier between the BODIPY derivatives with and without methyl groups (8.1 and 7.5 kcal/mol, respectively). Importantly, we noticed a 17-fold decrease in fluorescence lifetime observed with the **3-Ph** (0.8 ns) and **3-PhOMe** (0.8 ns) compared to **3-H** (12.1 ns) (see Figures S1−S4), which suggests the introduction of unproductive nonradiative decay pathways by the aryl substituents, possibly contributing to the unexpectedly lowered Φ_r in these compounds.

CONCLUSION

We have elucidated the effect of BODIPY PPG substituents on Φ_r at the boron, the 2-position, and the *meso*-methyl position. Although substituting the boron fluorines with inductively donating groups (e.g., Me and CH_2TMS) shows a ∼40−50-fold enhancement in the Φ_r, substituting the boron with a wide variety of other substituents has little effect on Φ_r despite

https://doi.org/10.1021/acs.joc.3c02980
J. Org. Chem. 2024, 89, 6740−6748

differences in the computed T_1 C−O heterolysis barrier. The lack of a correlation of the Φ_r with the computed bond breaking energy barrier for boron substitution suggests that the dominant effect on Φ_r is not the heterolysis rate constant and may be attributed to altering an "invisible" side photoreaction involving B−R bond scission. In contrast, when substituting the 2-position of the BODIPY PPG, there is a clear correlation between the computed C−O heterolysis barrier and the Φ_r. Electron-donating groups increase the efficiency of the photouncaging, whereas withdrawing groups attenuate it. For example, a 2-OH substituent increases Φ_r by ∼4-fold compared to the parent PPG. In contrast, withdrawing groups such as CHO diminish the Φ_r. Because the Φ_r correlates well with the computed C−O T_1 heterolysis barrier, these changes in Φ_r upon substitution likely derive from donating groups increasing the excited-state heterolysis rate and withdrawing groups slowing the excited-state heterolysis rate, with minimal differential impact on competing photochemical/photophysical channels. However, in contrast to prior reports showing that *meso*-methyl allyl substituents increase the photoreactivity, we find that *meso*-methyl aryl substituents do not increase the Φ_r, which we attribute to these groups introducing unproductive internal conversion channels that diminish the excited-state lifetime.

Overall, this work provides insights into how the photoreactivity of BODIPY PPGs can be tuned by substituents and shows the limits of using the computed excited-state heterolysis barrier to predict Φ_r. In cases where the substituents primarily impact the rate of the photoreaction, such as in the 2-position, the computed C−O heterolysis barrier can provide a useful tool for predicting Φ_r. However, in cases such as in the *meso*-methyl aryl substitution or boron substitution, where the substituents more greatly affect other photophysical/photochemical channels, the computed barrier is not a useful tool. Given that it is difficult *a priori* to predict the impact of a substituent on competing photochemical/photophysical channels, such a single-parameter approach may have limited utility, and new approaches may need to be developed.

EXPERIMENTAL SECTION

General Information. Reagents were purchased and used as received unless otherwise specified; when necessary, solvents were dried over activated molecular sieves for 1 day before use. **1-Me,**[19] **1-F,**[18] and **4**[26] were synthesized as previously reported. NMR spectra were recorded on Bruker NEO 400 (400 MHz) and Bruker AV III 600 (600 MHz). For Φ_r determinations, Bruker AV III 600 (600 MHz) was used. High-resolution mass spectra (HRMS) were obtained using a 6540 ESI-QTOF mass spectrometer (Agilent).

T_1 Heterolysis Barrier. Previous studies[19] indicate that the triplet state of the BODIPY photocage is a photoreactive state, as evidenced by higher quantum yields for derivatives bearing heavy atoms like iodine and because the Φ_r roughly doubles when the irradiated solution is first purged with inert gas compared to irradiations conducted under air.

All the structure optimizations and scans were performed using the Gaussian 09 software package[27] utilizing the B3LYP functional[28−30] and 6-31+G(d,p) polarized double-ζ basis set on triplet state with the SMD solvent model (water) at the default temperature (298.15 K). In all cases, optimized T_1 geometries were found to have zero imaginary frequencies.

A triplet state relaxed potential energy scan was conducted on the optimized geometries by increasing the C−O bond length by 0.1 Å. The difference in the SCF energies of the starting point and the point with the highest electronic energy on the curve was used for $\Delta E^{\ddagger}$.

Light Sources. For quantum yields of release determinations, a Luzchem LED illuminator (distance to sample: 3.8 cm) with a mounted cuvette holder and stir bar was used. Samples were irradiated with LEDi-RGB green light centered at 525 nm.

Quantum Yield Determination. All of the quantum yield experiments were carried out in a solvent mixture of 1:1 deuterated methanol and chloroform with **1-F** as the actinometer. The release of the leaving group, acetic acid, or chloroacetic acid was tracked using quantitative ^{1}H NMR (Figure S3). For quantitative accuracy, a 90° pulse angle was used along with 10 s of recycling delay cycle and eight scans. Approximately 1 mM solutions of the compounds were prepared, and absorbance of the solution at 532 nm was measured to ensure that absorbance is above 2 so that we could assume 100% light absorption by the sample. Three milliliters of the sample was irradiated in a cuvette using the LED illuminator green 466−538 nm (centered at 532 nm). After the irradiation, 0.6 mL of the sample was transferred to take the ^{1}H NMR spectrum. The sample from the NMR tube was then transferred back to the cuvette, and the irradiation process was continued. Dimethyl sulfone (1 mM) was used as the internal standard, and the release of acetic acid was determined to be relative to this internal standard. Commercially available deuterated methanol has impurities that appear around 1.9 ppm, close to the acetic acid peak, so the sample was irradiated for 5 min at the beginning to see a linear increment. Three trials with at least five data points were collected for each compound, and time was plotted against the concentration of the leaving group. An example graph can be found in the SI (Figure S2). The average of slopes from three trials was taken to get the final value of the quantum yield of the corresponding compound. The Φ_r for the compounds was determined using the following formula:

$$\Phi_r = \frac{\text{slope of the compound of interest}}{\text{slope of } \mathbf{1-F}} \times \Phi_r \text{ of } \mathbf{1-F}$$

Fluorescence Lifetime Measurements. Fluorescence lifetime (τ_{Fl}) measurements were carried out by measuring the fluorescence decay with a time-correlated single-photon counting (TCSPC) spectrometer (DeltaFlex, modular fluorescence lifetime system, HORIBA Scientific) and a 360 nm LED emitter (DeltaDiode, HORIBA Scientific). Solutions of **3-H** (0.1 mM), **3-Ph** (0.2 mM), and **3-PhOMe** (0.2 mM) in DCM were used, and the samples were excited with 540, 550, and 560 nm, respectively. The decays were fitted to the sum of exponential functions with iterative reconvolution by the WzTime software (Figure S4 and Table S1)

Synthetic Procedures and Characterizations. *1-CH_2TMS.* **1-F** (100 mg, 0.312 mmol, 1 equiv) was dissolved in 15 mL of dry dichloromethane (DCM) under a nitrogen atmosphere to which was added boron trichloride (37 mg, 0.312 mmol, 1 equiv). (Trimethylsilyl)methylmagnesium chloride (1 mL, excess) was then added. The solution was stirred at room temperature for 2 h. The reaction was quenched with water, washed once with saturated ammonium chloride solution and once with brine, and dried over sodium sulfate. The solvent was removed under a vacuum, and the crude mixture was purified with silica gel column chromatography using 30% ethyl acetate in hexanes as the eluent to give 46 mg of **1-CH_2TMS** as an orange solid (32%). ^{1}H NMR (400 MHz, $CDCl_3$) δ: 6.04 (2H, s), 5.38 (2H, s), 2.49 (6H, s), 2.37 (6H, s), 2.11 (3H, s), 0.14 (4H, s), −0.54 (18H, s). ^{13}C{^{1}H} NMR (400 MHz, $CDCl_3$) δ: 170.6, 153.2, 137.3, 133.7, 131.6, 123.0, 58.5, 20.4, 17.1, 15.8, −0.5. HRMS (ESI-QTOF) m/z $[M + H]^+$ calculated for $C_{24}H_{41}BN_2O_2Si_2$ 457.2872; found 457.2874.

1-BTA. **1-F** (100 mg, 0.312 mmol, 1 equiv) was dissolved in 15 mL of dry DCM under a nitrogen atmosphere to which was added boron trichloride (37 mg, 0.312 mmol, 1 equiv). A drop of triethylamine was then added followed by adding 1-(trimethylsilyl)-1*H*-benzotriazole (1 mL, excess). The solution was stirred at room temperature overnight. The reaction was washed once with saturated ammonium chloride solution and once with brine and dried over sodium sulfate. The solvent was removed under a vacuum, and the crude mixture was purified with silica gel column chromatography using 30% ethyl acetate in hexanes as the eluent to give 66 mg of **1-BTA** as an orange solid (41%). ^{1}H NMR (400 MHz, $CDCl_3$) δ 8.13 (2H, d, J = 8), δ 7.28 (5H, m), δ 6.31 (2H, d, J = 8.4), δ 6.17 (2H, s), δ 5.35 (2H, s), δ 2.44 (6H, s), δ 2.13 (3H, s), δ

https://doi.org/10.1021/acs.joc.3c02980
J. Org. Chem. 2024, 89, 6740−6748

1.60 (6H, s). $^{13}C\{^1H\}$ NMR (400 MHz, $CDCl_3$) δ: 170.1, 159.0, 143.1, 136.9, 134.8, 133.1, 127.1, 125.6, 124.5, 123.3, 119.3, 111.2, 57.6, 20.3, 15.6, 15.2. HRMS (ESI-QTOF) m/z $[M + H]^+$ calcd for $C_{28}H_{27}BN_8O_2$ 519.2423; found 519.2418.

1-OMe. **1-F** (100 mg, 0.312 mmol, 1 equiv) was dissolved in 15 mL of dry tetrahydrofuran (THF) under a nitrogen atmosphere to which was added aluminum chloride (42 mg, 0.312 mmol, 1 equiv). Methanol (1 mL, excess) was then added. The solution was stirred at room temperature for 2 h. The solvent was removed under a vacuum, and the crude mixture was purified with silica gel column chromatography using 30% ethyl acetate in hexanes as the eluent to give 73 mg of **1-OMe** as an orange solid (69%). ^1H NMR (400 MHz, $CDCl_3$) δ 6.07 (2H, s), 5.30 (2H, s), 2.86 (6H, s), 2.52 (6H, s), 2.36 (6H, s), δ 2.14 (3H, s). $^{13}C\{^1H\}$ NMR (400 MHz, $CDCl_3$) δ: 170.6, 156.6, 139.4, 133.9, 132.7, 121.9, 58.2, 48.9, 29.5, 20.5, 15.6, 14.5. HRMS (ESI-QTOF) m/z $[M + H]^+$ calcd for $C_{18}H_{25}BN_2O_4$ 345.1985; found 345.1987.

1-Ph. **1-F** (100 mg, 0.312 mmol, 1 equiv) was dissolved in 15 mL of dry THF under a nitrogen atmosphere to which was added aluminum chloride (42 mg, 0.312 mmol, 1 equiv). Phenol (1 mL, excess) was then added. The solution was stirred at room temperature overnight. The solvent was removed under a vacuum, and the crude mixture was purified with silica gel column chromatography using 20% dichloromethane in hexanes as the eluent to give 91 mg of **1-Ph** as an orange solid (62%). ^1H NMR (600 MHz, $CDCl_3$) δ 7.06 (2H, d, J = 8.4), δ 7.05 (2H, d, J = 9.0), δ 6.77 (2H, tt, J = 7.2, 1.2), δ 6.56 (4H, dd, J = 7.2, 1.2), δ 5.98 (2H, s), δ 5.39 (2H, s), δ 2.50 (6H, s), δ 2.38 (6H, s), δ 2.17 (3H, s). $^{13}C\{^1H\}$ NMR (600 MHz, $CDCl_3$) δ: 170.4, 157.2, 156.3, 141.2, 133.4, 133.2, 128.9, 123.0, 119.4, 118.3, 57.8, 20.6, 15.8, 15.2. HRMS (ESI-QTOF) m/z $[M + H]^+$ calcd for $C_{28}H_{29}BN_2O_4$ 469.2293; found 469.2266.

1-OBn. **1-F** (100 mg, 0.312 mmol, 1 equiv) was dissolved in 15 mL of dry THF under a nitrogen atmosphere to which was added aluminum chloride (42 mg, 0.312 mmol, 1 equiv). Benzyl alcohol (1 mL, excess) was then added. The solution was stirred at room temperature until the starting material was consumed. The solvent was removed under a vacuum, and the crude mixture was purified with silica gel column chromatography using 30% ethyl acetate in hexanes as the eluent to give 86 mg of **1-OBn** as an orange red solid (56%). ^1H NMR (600 MHz, $CDCl_3$) δ: 7.19 (10H, m), 6.04 (2H, s), 5.37 (2H, s), 4.14 (4H, s), 2.53 (6H, s), 2.43 (6H, s), 2.26 (3H, s). $^{13}C\{^1H\}$ NMR (600 MHz, $CDCl_3$) δ: 170.6, 157.0, 141.4, 139.7, 133.8, 132.7, 127.6, 127.3, 126.2, 122.2, 64.2 58.2, 20.6,15.6, 15.0. HRMS (ESI-QTOF) m/z $[M]^+$ calcd for $C_{30}H_{33}BN_2O_4$ 496.2528; found 496.2507. (5.24)

1-Cat. **1-F** (100 mg, 0.312 mmol, 1 equiv) was dissolved in 15 mL of anhydrous THF under a nitrogen atmosphere to which was added aluminum chloride (42 mg, 0.312 mmol, 1 equiv). Catechol (183 mg, 0.468 mmol, 1.5 equiv) was then added. The solution was stirred at room temperature overnight. The solvent was removed under a vacuum, and the crude mixture was purified with silica gel column chromatography using 30% ethyl acetate in hexanes as the eluent to give 85 mg of **1-Cat** as an orange solid (70%). ^1H NMR (600 MHz, $CDCl_3$) δ 6.76 (4H, m), 6.05 (2H, s), 5.32 (2H, s), 2.36 (6H, s), 2.14 (3H, s), 2.06 (6H, s). $^{13}C\{^1H\}$ NMR (600 MHz, $CDCl_3$) δ: 170.5, 158.4, 151.6, 141.9, 133.4, 123.4, 119.5, 108.7, 57.8, 29.7, 20.5, 15.7, 15.2. HRMS (ESI-QTOF) m/z $[M + H]^+$ calcd for $C_{22}H_{23}BN_2O_4$ 391.1829; found 391.1829.

1-PAA. **1-F** (100 mg, 0.312 mmol, 1 equiv) was dissolved in 15 mL of dry DCM under a nitrogen atmosphere to which was added boron trichloride (37 mg, 0.312 mmol, 1 equiv). One drop of triethylamine was then added followed by phenylacetic acid (106 mg, 0.78 mmol, 2.5 equiv). The solution was stirred at room temperature for 2 h. The reaction mixture was washed once with saturated sodium bicarbonate solution and once with brine and dried over sodium sulfate. The solvent was removed under a vacuum, and the crude mixture was purified with silica gel column chromatography using 30% ethyl acetate in hexane as the eluent to give 90 mg of **1-PAA** as an orange solid (53%). ^1H NMR (600 MHz, $CDCl_3$) δ 7.32 (4H, t, J = 7.2), δ 7.27 (2H, d, J = 6.6), δ 7.24 (4H, d, J = 7.8), δ 6.06 (2H, s), δ 5.35 (2H, s), δ 3.55 (4H, s), δ 2.40 (6H, s), 2.16 (9H, s). $^{13}C\{^1H\}$ NMR (600 MHz, $CDCl_3$) δ: 171.1, 170.5, 154.7, 141.2, 135.3, 134.1, 134.0, 129.4, 128.3, 126.7, 122.2, 58.0, 43.1, 20.5, 15.6, 14.2. HRMS (ESI-QTOF) m/z $[M + H]^+$ calcd for $C_{32}H_{33}BN_2O_6$ (553.2510); found 553.2485.

1-CN. **1-F** (500 mg, 1.57 mmol, 1 equiv) was dissolved in 15 mL of dry DCM under a nitrogen atmosphere to which was added tin tetrachloride (0.8 mL, 6.84 mmol, 4.4 equiv). Trimethylsilyl cyanide (2 mL, excess) was then added. The solution was stirred 4 h at room temperature until the starting material was consumed and then was quenched with water. The residue was extracted with dichloromethane, washed with saturated sodium bicarbonate solution and once with brine, and dried over sodium sulfate. The solvent was removed under a vacuum, and the crude mixture was purified with silica gel column chromatography using 35% ethyl acetate in hexanes as the eluent to give 400 mg of **1-CN** as an orange solid (76%). ^1H NMR (600 MHz, $CDCl_3$) δ: 6.28 (2H, s), δ5.32 (2H, s), δ 2.72 (6H, s), δ 2.42 (6H, s), δ 2.16 (3H, s). $^{13}C\{^1H\}$ NMR (400 MHz, $CDCl_3$) δ: 170.0, 156.8, 142.6, 134.3, 130.7, 126.8, 126.1, 125.3, 124.6, 123.5, 57.1, 20.2, 15.6, 15.3. HRMS (ESI-QTOF) m/z $[M-H]^-$ calcd for $C_{18}H_{19}BN_4O_2$ 333.1522; found 333.1538.

2-CHO. A portion of phosphorus oxychloride ($POCl_3$) (12.0 mL) was added dropwise to an ice-cold solution of dimethylformamide (DMF) (12.0 mL). The solution was allowed to come to room temperature, and a solution of **1-F** (0.40 g, 1.25 mmol) in dichloroethane DCE (20 mL). The reaction mixture was stirred for 4 h. Upon completion of the reaction, the reaction was cooled to 0 °C, and saturated sodium bicarbonate (50 mL) was added. The reaction mixture was stirred for 30 min, and then the aqueous layer was extracted thrice with DCM. The organic layer was washed with brine and dried over anhydrous sodium sulfate. After the organic layer was concentrated under a vacuum, it was loaded onto a silica gel column and flushed with 20−30% ethyl acetate in hexanes to yield **2-CHO** as a bright orange solid (0.33 g, 77%). ^1H NMR (600 MHz, $CDCl_3$) δ: 10.11 (s, 1H), 6.28 (s, 1H), 5.37 (s, 2H), 2.79 (s, 3H), 2.66 (s, 3H), 2.61 (s, 3H), 2.44 (s, 3H), 2.15 (s, 3H). $^{13}C\{^1H\}$ NMR (151 MHz, $CDCl_3$) δ: 186.0, 170.3, 163.5, 157.2, 145.8, 140.7, 135.6, 130.6, 125.5, 57.5, 20.6, 16.3, 15.3, 12.9, 12.2. HRMS (ESI-QTOF) m/z $[M]^+$ calcd for $C_{17}H_{19}BF_2N_2O_3$ $[M]^+$ 349.1535; 349.1536 found.

2-OCOH. To a solution of compound **2-CHO** (0.450 g, 1.29 mmol, 1 equiv) in DCM (15 mL) were added meta chloroperbenzoic acid (0.875 g, 5.7 mmol, 4 equiv) and sodium bicarbonate (0.87 g, 10.32 mmol, 8 equiv). The reaction was stirred at room temperature for 1 h. The reaction mixture was then concentrated under a vacuum, loaded onto a silica gel column, and flushed with 20−30% ethyl acetate in hexanes to yield **2-OCOH** as a pink solid (0.245 g, 52%). ^1H NMR (600 MHz, $CDCl_3$) δ: 8.26 (s, 1H), 6.13 (s, 1H), 5.29 (s, 2H), 2.55 (s, 3H), 2.41 (s, 3H), 2.38 (s, 3H), 2.18 (s, 3H), 2.14 (s, 3H). $^{13}C\{^1H\}$ NMR (101 MHz, $CDCl_3$) δ: 170.6, 159.8, 158.4, 145.9, 143.5, 140.3, 134.4, 133.8, 128.7, 128.3, 123.4, 57.9, 29.8, 20.7, 16.0, 15.1, 11.5, 11.2. HRMS (ESI-QTOF) m/z $[M + H]^+$ calcd for $C_{17}H_{19}BF_2N_2O_4$ 365.1484; found 365.1477.

2-OH. A catalytic amount of sodium methoxide (0.014 g, 0.0003 mmol, 0.04 equiv) was added to a solution of **2-OCOH** (0.245 g, 0.673 mmol, 1 equiv) in DCM and methanol mixture (1:1) and stirred for 3 h. Upon completion of the reaction, the reaction mixture was concentrated under a vacuum and was purified using flash column chromatography with 30% ethyl acetate in hexanes as the eluent. **2-OH** was obtained as a purple solid (0.090 g, 40%).^1H NMR (600 MHz, $CDCl_3$) δ 6.02 (s, 1H), 5.26 (s, 2H), 4.00 (s, 1H), 2.51 (d, J = 6.2 Hz, 6H), 2.33 (s, 3H), 2.22 (s, 3H), 2.13 (s, 3H). $^{13}C\{^1H\}$ NMR (151 MHz, $CDCl_3$) δ: 170.8, 155.2, 147.3, 140.1, 132.5, 132.1, 130.2, 121.7, 121.3, 58.2, 20.8, 15.6, 14.7, 11.3, 10.6. HRMS (ESI-QTOF) m/z $[M + H]^+$ calcd for $C_{16}H_{19}BF_2N_2O_3$ 337.1535; found 337.1535.

2-OMe. To a solution of **2-OH** (0.10 g, 0.287 mmol, 1 equiv) in acetone (20 mL), potassium carbonate (0.476 g, 3.446 mmol, 12 equiv) followed by methyl iodide (0.08 mL, 1.285 mmol, 4 equiv) was added and stirred at room temperature for 2 h. Upon completion of the reaction, the reaction mixture was concentrated under a vacuum and was purified using flash column chromatography with 20−30% ethyl acetate in hexanes as the eluent. **2-OMe** was obtained as a purple solid (0.080 g, 80%).^1H NMR (600 MHz, $CDCl_3$) δ 6.05 (s, 1H), 5.27 (s, 2H), 3.73 (s, 3H), 2.52 (s, 6H), 2.34 (s, 3H), 2.26 (s, 3H), 2.13 (s, 3H).

https://doi.org/10.1021/acs.joc.3c02980
J. Org. Chem. 2024, 89, 6740−6748

$^{13}C\{^1H\}$ NMR (151 MHz, $CDCl_3$) δ: 170.7, 156.5, 150.0, 133.3, 128.4, 121.9, 62.3, 58.1, 29.8, 20.8, 15.7, 14.8, 11.6, 10.8. HRMS (ESI-QTOF) m/z $[M]^+$ calcd for $C_{17}H_{22}BF_2N_2O_3$ 351.1691; found 351.1692.

2-CH=C(CN)$_2$. Compound **2-CHO** (0.350 g, 1 mmol, 1 equiv) and malononitrile (73 mg, 1.1 mmol, 1.1 equiv) were dissolved in DCM followed by the addition of aluminum oxide (0.450 g, 4.4 mmol, 4.4 equiv). The reaction mixture was stirred at room temperature until all of the starting material was consumed. The solid was removed by filtering through Celite, and the solution was concentrated under a vacuum and then purified with flash column chromatography using 30% ethyl acetate in hexanes as eluent to afford **2-CH=C(CN)$_2$** as a bright orange solid (0.340 g, 86%) (^1H NMR (600 MHz, $CDCl_3$) δ 7.78 (s, 1H), 6.31 (s, 1H), 5.36 (s, 2H), 2.62 (s, 3H), 2.61 (s, 3H), 2.45 (s, 3H), 2.42 (s, 3H), 2.15 (s, 3H). $^{13}C\{^1H\}$ NMR (151 MHz, $CDCl_3$) δ: 170.3, 165.0, 153.5, 153.0, 146.8, 137.1, 136.6, 135.0, 132.0, 126.2, 114.3, 113.2, 83.6, 57.7, 20.7, 16.5, 15.6, 15.3, 14.4, 14.4. HRMS (ESI-QTOF) m/z $[M-H]^-$ calcd for $C_{20}H_{19}BF_2N_4O_2$ 395.1491; found 395.1461.

Compound 5. Sodium periodate (1.16 g, 5.5 mmol, 2.5 equiv) was added to a solution of **4** (0.70 g, 2.2 mmol, 1 equiv) in 60:40 THF (100 mL). The reaction mixture was stirred until all the starting material was consumed (typically an overnight reaction). Upon completion, THF was removed under a vacuum, and product was extracted with DCM followed by washing with brine and drying over anhydrous sodium sulfate. The organic phase was then concentrated under a vacuum and purified via column chromatography (10−30% ethyl acetate in hexanes) to afford **5** as a pink solid (0.425 g, 70%). ^1H NMR (400 MHz, $CDCl_3$) δ 10.57 (s, 1H), 6.08 (s, 2H), 2.54 (s, 6H), 2.13 (s, 6H).$^{13}C\{^1H\}$ NMR (101 MHz, $CDCl_3$) δ 193.2, 158.6, 141.6, 136.2, 128.9, 122.0, 15.5, 15.0. HRMS (ESI-QTOF) m/z $[M + H]^+$ calcd for $C_{14}H_{15}BF_2N_2O$ 277.1323; found 277.1320.

General Procedure for Grignard Reaction. The respective Grignard reagent (2 equiv) was added slowly to an ice-cold solution of compound **5** in anhydrous DCM under N_2 and stirred until the starting material disappeared by TLC (~3−4 h). The reaction was then quenched with water, and the organic layer was washed with saturated ammonium chloride and brine separately. The solution was dried over anhydrous sodium sulfate, concentrated under a vacuum, and purified using flash column chromatography (hexanes: ethyl acetate gradient).

3-Ph OH. Phenylmagnesium bromide (0.5 M, 1.44 mL, 0.72 mmol, 2 equiv) was reacted with compound **5** (100 mg, 0.36 mmol, 1 equiv) following the general procedure to afford an orange solid (83 mg, 65%). ^1H NMR (600 MHz, $CDCl_3$) δ: 7.45 (d, J = 8.4 Hz, 2H), 7.34 (t, J = 7.4 Hz, 2H), 7.30 (t, J = 7.2 Hz, 1H), 6.65 (s, 1H), 6.03 (s, 2H), 2.55 (s, 6H), 2.03 (s, 6H). $^{13}C\{^1H\}$ NMR (151 MHz, $CDCl_3$) δ: 144.5, 139.3, 132.1, 129.9, 128.7, 128.0, 126.5, 122.8, 69.5, 29.8, 17.3, 14.8. HRMS (ESI-QTOF) m/z $[M + H]^+$ calcd for $C_{20}H_{21}BF_2N_2O$ 355.1793; found 355.1796 found.

3-PhOMe OH. 4-Methoxyphenylmagnesium bromide (0.5 M, 1.44 mL, 0.72 mmol, 2 equiv) was reacted with compound 9 (100 mg, 0.36 mmol, 1 equiv) following the general procedure to give an orange solid (108 mg, 78%). ^1H NMR (600 MHz, $CDCl_3$) δ: 7.34 (m, 2H), 6.86 (d, J = 8.8 Hz, 2H), 6.57 (s, 1H), 6.02 (s, 2H), 3.79 (s, 3H), 2.54 (s, 6H), 2.04 (s, 6H). $^{13}C\{^1H\}$ NMR (151 MHz, $CDCl_3$) δ: 159.3, 144.9, 132.0, 131.3, 127.9, 122.7, 114.0, 69.3, 55.4, 14.8. HRMS (ESI-QTOF) m/z $[M + H]^+$ calcd for $C_{21}H_{23}BF_2N_2O_2$ 385.1898, found 385.1899.

General Procedure for Attaching Chloroacetic Acid. *N,N′*-Dicyclohexylcarbodiimide (DCC) was slowly added to an ice-cold solution of chloroacetic acid, respective alcohol, and 4-dimethylaminopyridine in DCM at 0 °C. The reaction was stirred at room temperature for 2 h. The reaction mixture was filtered, and the filtrate was thoroughly washed with saturated sodium bicarbonate followed by drying over anhydrous sodium sulfate. The organic layer was then concentrated under a vacuum and purified with flash column chromatography.

3-Ph. DCC (69 mg, 0.34 mmol, 1.2 equiv), chloroacetic acid (30 mg, 0.31 mmol, 1.1 equiv), **3-Ph OH** (100 mg, 0.28 mmol, 1 equiv), and 4-dimethylaminopyridine (0.4 mg, 0.003 mmol, 0.011 equiv) were reacted according to the general procedure followed by flash column chromatography (5−20% ethyl acetate in hexanes) to afford **3-Ph** as an orange solid (60 mg, 50%). ^1H NMR (600 MHz, $CDCl_3$) δ: 7.91 (s, 1H), 7.39−7.29 (m, 5H), 6.11 (s, 1H), 6.00 (s, 1H), 4.23−4.13 (dd, 2H), 2.55 (s, 6H), 2.37 (s, 3H), 1.84 (s, 3H). $^{13}C\{^1H\}$ NMR (151 MHz, $CDCl_3$) δ: 167.1, 157.1, 156.5, 143.2, 143.0, 135.7, 129.1, 128.8, 126.4, 123.1, 71.4, 40.9, 17.0, 14.9. HRMS (ESI-QTOF) m/z $[M + H]^+$ calcd for $C_{22}H_{22}BClF_2N_2O_2$ 431.1510; found 431.1517.

3-PhOMe. DCC (58 mg, 0.17 mmol, 1.2 equiv), chloroacetic acid (24 mg, 0.15 mmol, 1.1 equiv), **3-PhOMe OH** (90 mg, 0.14 mmol, 1 equiv), and 4-dimethylaminopyridine (0.3 mg, 0.002 mmol, 0.011 equiv) were reacted according to the general procedure followed by flash column chromatography (5−30% ethyl acetate in hexanes) to afford **3-PhOMe** as an orange solid (45 mg, 70%). ^1H NMR (600 MHz, $CDCl_3$) δ: 7.84 (s, 1H), 7.24 (d, J = 8.3 Hz, 2H), 6.88 (d, J = 8.8 Hz, 2H), 6.10 (s, 1H), 6.01 (s, 1H), 4.19−4.11 (m, 2H), 3.80 (s, 3H), 2.55 (s, 6H), 2.35 (s, 3H), 1.89 (s, 3H). $^{13}C\{^1H\}$ NMR (151 MHz, $CDCl_3$) δ: 167.1, 160.0, 157.1, 156.4, 137.6, 132.4, 128.1, 127.4, 123.1, 114.4, 71.4, 55.4, 41.0, 17.2, 16.9, 14.9. HRMS (ESI-QTOF) m/z $[M + H]^+$ calcd for $C_{23}H_{24}BClF_2N_2O_3$ 461.1615; found 461.1629.

3-H. DCC (223 mg, 1.08 mmol, 1.2 equiv), chloroacetic acid (93 mg, 0.99 mmol, 1.1 equiv), **1-F OH** (250 mg, 0.9 mmol, 1 equiv), and 4-dimethylaminopyridine (0.1 mg, 0.001 mmol, 0.011 equiv) were reacted according to the general procedure followed by flash column chromatography (10−30% ethyl acetate in hexanes) to afford **3-H** as an orange solid (86 mg, 27%). ^1H NMR (600 MHz, $CDCl_3$) δ 6.09 (s, 2H), 5.42 (s, 2H), 4.10 (s, 2H), 2.53 (s, 6H), and 2.36 (s, 6H). $^{13}C\{^1H\}$ NMR (151 MHz, $CDCl_3$) δ: 167.2, 157.1, 141.6, 132.7, 132.0, 122.7, 59.3, 40.5, 15.8, 14.8. HRMS (ESI-QTOF) m/z $[M + H]^+$ calcd for $C_{16}H_{18}BClF_2N_2O_2$ 355.1196; found 355.1196.

■ ASSOCIATED CONTENT

Data Availability Statement

The data underlying this study are available in the published article and its Supporting Information.

Supporting Information

The Supporting Information is available free of charge at https://pubs.acs.org/doi/10.1021/acs.joc.3c02980.

Spectral data (^1H NMR, $^{13}C\{^1H\}$ NMR, HRMS) for the newly synthesized compounds, quantum yield details, computational coordinates, and absolute energies (PDF)

■ AUTHOR INFORMATION

Corresponding Author

Arthur H. Winter − *Department of Chemistry, Iowa State University, Ames, Iowa 50010, United States;* orcid.org/0000-0003-2421-5578; Email: winter@iastate.edu

Authors

Komadhie C. Dissanayake − *Department of Chemistry, Iowa State University, Ames, Iowa 50010, United States;* orcid.org/0000-0003-3347-1004

Ding Yuan − *Department of Chemistry, Iowa State University, Ames, Iowa 50010, United States*

Complete contact information is available at: https://pubs.acs.org/10.1021/acs.joc.3c02980

Author Contributions

‡K.C.D. and D.Y. contributed equally.

Funding

NSF CHE-2055335, Research Corporation Cottrell SEED Award, and NIH R21GM151612

Notes

The authors declare no competing financial interest.

■ ACKNOWLEDGMENTS

We thank the NSF, Research Corporation, and NIH for the support.

■ REFERENCES

(1) Klán, P.; Šolomek, T.; Bochet, C. G.; Blanc, A.; Givens, R.; Rubina, M.; Popik, V.; Kostikov, A.; Wirz, J. Photoremovable Protecting Groups in Chemistry and Biology: Reaction Mechanisms and Efficacy. *Chem. Rev.* **2013**, *113* (1), 119−191.
(2) Ellis-Davies, G. C. R. Caged Compounds: Photorelease Technology for Control of Cellular Chemistry and Physiology. *Nat. Methods* **2007**, *4* (8), 619−628.
(3) Adams, S. R.; Tsien, R. Y. Controlling Cell Chemistry with Caged Compounds. *Annu. Rev. Physiol.* **1993**, *55* (1), 755−784.
(4) Specht, A.; Bolze, F.; Omran, Z.; Nicoud, J.; Goeldner, M. Photochemical Tools to Study Dynamic Biological Processes. *HFSP Journal* **2009**, *3* (4), 255−264.
(5) Weinstain, R.; Slanina, T.; Kand, D.; Klán, P. Visible-to-NIR-Light Activated Release: From Small Molecules to Nanomaterials. *Chem. Rev.* **2020**, *120* (24), 13135−13272.
(6) Anderson, J. C.; Reese, C. B. A Photo-Induced Rearrangement Involving Aryl Participation. *Tetrahedron Lett.* **1962**, *3* (1), 1−4.
(7) Park, C.-H.; Givens, R. S. New Photoactivated Protecting Groups. 6. p-Hydroxyphenacyl: A Phototrigger for Chemical and Biochemical Probes1,2. *J. Am. Chem. Soc.* **1997**, *119* (10), 2453−2463.
(8) Kaplan, J. H.; Ellis-Davies, G. C. Photolabile Chelators for the Rapid Photorelease of Divalent Cations. *Proc. Natl. Acad. Sci. U. S. A.* **1988**, *85* (17), 6571−6575.
(9) Engels, J.; Schlaeger, E. J. Synthesis, Structure, and Reactivity of Adenosine Cyclic 3′,5′-Phosphate Benzyl Triesters. *J. Med. Chem.* **1977**, *20* (7), 907−911.
(10) Givens, R. S.; Matuszewski, B. Photochemistry of Phosphate Esters: An Efficient Method for the Generation of Electrophiles. *J. Am. Chem. Soc.* **1984**, *106* (22), 6860−6861.
(11) Shrestha, P.; Kand, D.; Weinstain, R.; Winter, A. H. Meso-Methyl BODIPY Photocages: Mechanisms, Photochemical Properties, and Applications. *J. Am. Chem. Soc.* **2023**, *145* (32), 17497−17514.
(12) Digby, E. M.; Ayan, S.; Shrestha, P.; Gehrmann, E. J.; Winter, A. H.; Beharry, A. A. Photocaged DNA-Binding Photosensitizer Enables Photocontrol of Nuclear Entry for Dual-Targeted Photodynamic Therapy. *J. Med. Chem.* **2022**, *65* (24), 16679−16694.
(13) Shrestha, P.; Mukhopadhyay, A.; Dissanayake, K. C.; Winter, A. H. Efficiency of Functional Group Caging with Second-Generation Green- and Red-Light-Labile BODIPY Photoremovable Protecting Groups. *J. Org. Chem.* **2022**. *8*714334.
(14) Contreras-García, E.; Lozano, C.; García-Iriepa, C.; Marazzi, M.; Winter, A. H.; Torres, C.; Sampedro, D. Controlling Antimicrobial Activity of Quinolones Using Visible/NIR Light-Activated BODIPY Photocages. *Pharmaceutics* **2022**, *14* (5), 1070.
(15) Leichnitz, S.; Dissanayake, K. C.; Winter, A. H.; Seeberger, P. H. Photo-Labile BODIPY Protecting Groups for Glycan Synthesis. *Chem. Commun.* **2022**, *58* (75), 10556−10559.
(16) Peterson, J. A.; Fischer, L. J.; Gehrmann, E. J.; Shrestha, P.; Yuan, D.; Wijesooriya, C. S.; Smith, E. A.; Winter, A. H. Direct Photorelease of Alcohols from Boron-Alkylated BODIPY Photocages. *J. Org. Chem.* **2020**, *85* (8), 5712−5717.
(17) Rubinstein, N.; Liu, P.; Miller, E. W.; Weinstain, R. Meso-Methylhydroxy BODIPY: A Scaffold for Photo-Labile Protecting Groups. *Chem. Commun.* **2015**, *51* (29), 6369−6372.
(18) Goswami, P. P.; Syed, A.; Beck, C. L.; Albright, T. R.; Mahoney, K. M.; Unash, R.; Smith, E. A.; Winter, A. H. BODIPY-Derived Photoremovable Protecting Groups Unmasked with Green Light. *J. Am. Chem. Soc.* **2015**, *137* (11), 3783−3786.
(19) Slanina, T.; Shrestha, P.; Palao, E.; Kand, D.; Peterson, J. A.; Dutton, A. S.; Rubinstein, N.; Weinstain, R.; Winter, A. H.; Klán, P. In Search of the Perfect Photocage: Structure−Reactivity Relationships in Meso-Methyl BODIPY Photoremovable Protecting Groups. *J. Am. Chem. Soc.* **2017**, *139* (42), 15168−15175.
(20) Shrestha, P.; Dissanayake, K. C.; Gehrmann, E. J.; Wijesooriya, C. S.; Mukhopadhyay, A.; Smith, E. A.; Winter, A. H. Efficient Far-Red/Near-IR Absorbing BODIPY Photocages by Blocking Unproductive Conical Intersections. *J. Am. Chem. Soc.* **2020**, *142* (36), 15505−15512.
(21) Schulte, A. M.; Alachouzos, G.; Szymański, W.; Feringa, B. L. Strategy for Engineering High Photolysis Efficiency of Photocleavable Protecting Groups through Cation Stabilization. *J. Am. Chem. Soc.* **2022**, *144* (27), 12421−12430.
(22) Wijesooriya, C. S.; Peterson, J. A.; Shrestha, P.; Gehrmann, E. J.; Winter, A. H.; Smith, E. A. A Photoactivatable BODIPY Probe for Localization-Based Super-Resolution Cellular Imaging. *Angew. Chem., Int. Ed.* **2018**, *57* (39), 12685−12689.
(23) Umeda, N.; Takahashi, H.; Kamiya, M.; Ueno, T.; Komatsu, T.; Terai, T.; Hanaoka, K.; Nagano, T.; Urano, Y. Boron Dipyrromethene As a Fluorescent Caging Group for Single-Photon Uncaging with Long-Wavelength Visible Light. *ACS Chem. Biol.* **2014**, *9* (10), 2242−2246.
(24) Chung, K.-Y.; Page, Z. A. Boron-Methylated Dipyrromethene as a Green Light Activated Type I Photoinitiator for Rapid Radical Polymerizations. *J. Am. Chem. Soc.* **2023**, *145* (32), 17912−17918.
(25) Kand, D.; Liu, P.; Navarro, M. X.; Fischer, L. J.; Rousso-Noori, L.; Friedmann-Morvinski, D.; Winter, A. H.; Miller, E. W.; Weinstain, R. Water-Soluble BODIPY Photocages with Tunable Cellular Localization. *J. Am. Chem. Soc.* **2020**, *142* (11), 4970−4974.
(26) Palao-Utiel, E.; Montalvillo-Jiménez, L.; Esnal, I.; Prieto-Montero, R.; Agarrabeitia, A. R.; García-Moreno, I.; Bañuelos, J.; López-Arbeloa, I.; de la Moya, S.; Ortiz, M. J. Controlling Vilsmeier-Haack Processes in Meso-methylBODIPYs: A New Way to Modulate Finely Photophysical Properties in Boron Dipyrromethenes. *Dyes Pigm.* **2017**, *141*, 286−298.
(27) Frisch, M. J.; Trucks, G. W.; Schlegel, H. B.; Scuseria, G. E.; Robb, M. A.; Cheeseman, J. R.; Scalmani, G.; Barone, V.; Mennucci, B.; Petersson, G. A.; Nakatsuji, H.; Caricato, M.; Li, X.; Hratchian, P. H.; Izmaylov, A. F.; Bloino, J.; Zheng, G.; Sonnenberg, J. L.; Hada, M.; Ehara, M.; Toyota, K.; Fukuda, R.; Hasegawa, J.; Ishida, M.; Nakajima, T.; Honda, Y.; Kitao, O.; Nakai, H.; Vreven, T.; Montgomery, J. A., Jr.; Peralta, E.; Ogliaro, F.; Bearpark, M.; Heyd, J.; Brothers, E.; Kudin, K. N.; Staroverov, V. N.; Kobayashi, R.; Normand, J.; Raghavachari, K.; Rendell, A.; Burant, J. C.; Iyengar, S. S.; Tomasi, J.; Cossi, M.; Rega, N.; Millam, J. M.; Klene, M.; Knox, J. E.; Cross, J. B.; Bakken, V.; Adamo, C.; Jaramillo, J.; Gomperts, R.; Stratmann, R. E.; Yazyev, O.; Austin, A. J.; Cammi, R.; Pomelli, C.; Ochterski, J. W.; Martin, R. L.; Morokuma, K.; Zakrzewski, V. G.; Voth, G. A.; Salvador, P.; Dannenberg, J. J.; Dapprich, S.; Daniels, A. D.; Farkas, O.; Foresman, J. B.; Ortiz, J. V.; Cioslowski, J.; Fox, D. J. *Gaussian 09*; Gaussian, Inc.: Wallingford, CT, 2009.
(28) Lee, C.; Yang, W.; Parr, R. G. Development of the Colle-Salvetti Correlation-Energy Formula into a Functional of the Electron Density. *Phys. Rev. B* **1988**, *37* (2), 785−789.
(29) Becke, A. D. Density-functional Thermochemistry. III. The Role of Exact Exchange. *J. Chem. Phys.* **1993**, *98* (7), 5648−5652.
(30) Stephens, P. J.; Devlin, F. J.; Ashvar, C. S.; Chabalowski, C. F.; Frisch, M. J. Theoretical Calculation of Vibrational Circular Dichroism Spectra. *Faraday Discuss.* **1994**, *99* (0), 103−119.

https://doi.org/10.1021/acs.joc.3c02980
J. Org. Chem. 2024, 89, 6740−6748